OTF compensation in structured illumination superresolution images

Sapna A. Shroff*[a,b,c], James R. Fienup,[b,c,a] and David R. Williams[b,c]
[a]Electrical and Computer Engineering, University of Rochester, Rochester, NY 14627, USA;
[b]Institute of Optics, University of Rochester, Rochester, NY 14627, USA;
[c]Center for Visual Science, University of Rochester, Rochester, NY 14627, USA

ABSTRACT

The lateral resolution of an imaging system is limited by its numerical aperture and the wavelength. Structured illumination incident on the object heterodynes the higher spatial frequencies of the object with the spatial frequency of the sinusoidal illumination into the passband of the imaging system providing lateral superresolution. This idea has been implemented in microscopy. Multiple images of an object are taken, with distinct phase shifts in the sinusoidally patterned illumination. They are processed to separate the conventional, un-aliased object spatial frequencies from the aliased ones, which contain superresolution information. The separated aliased terms are de-aliased (i.e. the spatial frequencies in them are moved to their correct locations in Fourier space) giving superresolution along the direction perpendicular to the orientation of the sinusoidal fringe pattern. This process is repeated with, say, 60° and 120° rotation of the sinusoidal fringe illumination to obtain superresolution in all directions. The final reconstructed image can be obtained by appropriate combination of the de-aliased superresolution components with the conventional, un-aliased components. We discuss the signal-to-noise ratio (SNR) and optical transfer function (OTF) compensation in the combination of all these components to obtain an image with lateral superresolution.

Keywords: Superresolution, structured illumination, moiré, aliasing, deconvolution, optical imaging, microscopy, image processing

1. INTRODUCTION

The resolution of any imaging system is limited by its numerical aperture and the wavelength. However these limits are valid only for the case of uniform, on-axis illumination and imaging linear fluorescence or transmission/reflection. Sinusoidally patterned illumination can be used to go beyond this limit on resolution.

The basic idea is that a sinusoidally patterned illumination incident on an object multiplies with it, producing a moiré, beat pattern. This moiré pattern heterodynes the high spatial frequencies of the object with the spatial frequency of the sinusoidal illumination and effectively shifts the high spatial frequencies of the object into the passband of the imaging system. This technique has been implemented in fluorescence microscopy to obtain either lateral superresolution or axial sectioning [1-21]. Multiple images of the object are taken with the phase of the sinusoidal pattern shifted by distinct amounts and the orientation of the sinusoidal illumination rotated a few times. These images are processed to extract the aliased, high frequencies to obtain a superresolved image. For the case of fluorescence imaging due to linear absorption and emission, up to 100% superresolution can be obtained.

Conventionally three images are taken with phase shifts of 0°, 120° and 240° in the sinusoidal illumination. We discuss a technique which will be valid for any number, N, of sinusoidally patterned images, where $N \geq 3$, and for equally spaced as well as randomly spaced phase shifts in the sinusoidal illumination. In this paper we discuss the effect of SNR and OTF compensation involved in the processing of these sinusoidally patterned images to obtain a superresolved reconstruction.

Unconventional Imaging IV, edited by Jean J. Dolne, Thomas J. Karr, Victor L. Gamiz,
Proc. of SPIE Vol. 7094, 709402, (2008) · 0277-786X/08/$18 · doi: 10.1117/12.791052

2. THEORY

2.1 Sinusoidally patterned image formation

We consider the case of incoherent imaging, such as for a fluorescent object illuminated by an incoherent source of illumination. The pattern is produced by a sinusoidal grating in the illumination path. Consider a sinusoidal illumination field, $U_s(x,y)=\cos(2\pi f_o x+\phi_n)$, having a spatial frequency $(f_o,0)$ and a phase shift of ϕ_n. The intensity of this sinusoidal illumination has twice this frequency, $(2f_o,0)$, and twice this phase shift, $2\phi_n$. Let us assume a modulation contrast factor, *m*, affecting the contrast of the sinusoidal component of this intensity to account for different efficiencies of gratings producing the sinusoidal patterned illumination. Then the intensity of this sinusoidal illumination is given by

$$I_s(x,y)=\frac{1}{2}\left[1+m\cos(4\pi f_o x+2\phi_n)\right]. \tag{1}$$

Let $\mathcal{G}_o$ be the Fourier transform of the object intensity and $\mathcal{H}_1$ and $\mathcal{H}_2$ be the optical transfer functions (OTFs) of the illumination and imaging paths, respectively. If the illumination and imaging paths are identical and the image is formed on a double-pass reflection from the object, then $\mathcal{H}_2(f_x,f_y)=\mathcal{H}_1(-f_x,-f_y)$ [22]. The Fourier transform, $\mathcal{G}_n$, of the image, given by [2,4,21], including measurement noise can be written as

$$\begin{aligned}\hat{\mathcal{G}}_n(f_x,f_y)&=\mathcal{G}_n(f_x,f_y)+N_n(f_x,f_y)\\&=\frac{1}{2}\mathcal{H}_1(0,0)\mathcal{H}_2(f_x,f_y)\mathcal{G}_o(f_x,f_y)+\frac{m}{4}\mathcal{H}_1(2f_o,0)e^{i2\phi_n}\mathcal{H}_2(f_x,f_y)\mathcal{G}_o(f_x-2f_o,f_y)\\&\quad+\frac{m}{4}\mathcal{H}_1(-2f_o,0)e^{-i2\phi_n}\mathcal{H}_2(f_x,f_y)\mathcal{G}_o(f_x+2f_o,f_y)+N_n(f_x,f_y).\end{aligned} \tag{2}$$

Ignoring noise for the moment, Eq. (2) indicates that the Fourier transform of this image, visualized in Figure 1, has three components, the unshifted object Fourier transform, $\mathcal{G}_o(f_x,f_y)$, and two shifted copies of the object Fourier transform, $\mathcal{G}_o(f_x-2f_o,f_y)$ and $\mathcal{G}_o(f_x+2f_o,f_y)$.

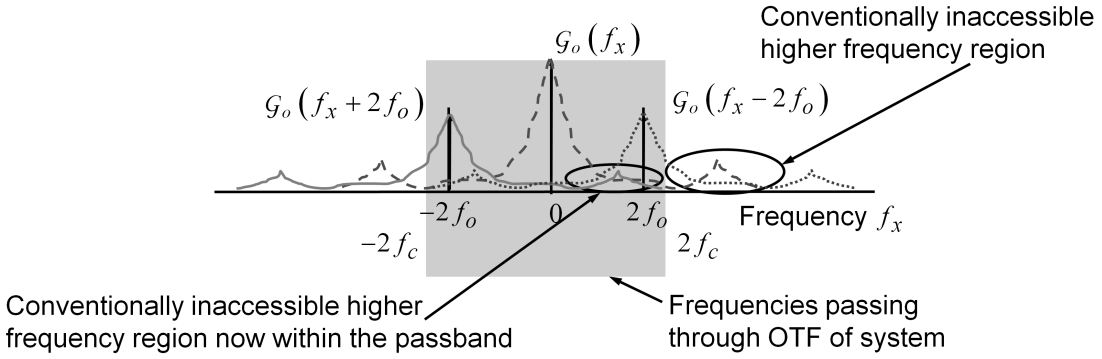

Figure 1. Visualization of structured illumination image in Fourier domain [21]

The shifted components carry portions of the object's Fourier transform that would ordinarily lie outside the passband of a conventional imaging system, and shift them into the passband of the conventional OTF,

making them accessible. In order to obtain a superresolved image, the three overlapping terms must be separated. The unshifted version may be retained as is, but the shifted versions must be moved in Fourier space so as to bring the spatial frequencies of these components from $\left(f_x - 2f_o, f_y\right)$ and $\left(f_x + 2f_o, f_y\right)$ coordinates back to the $\left(f_x, f_y\right)$ coordinates. Then all three components may be combined appropriately to obtain a superresolved image. Next we discuss the processing involved in obtaining these component images.

2.2 Processing to obtain superresolution components

Continuing to ignore the noise, we treat the three overlapping copies of the object's Fourier transform as three unknowns. In order to solve for three unknowns we need three or more images. Therefore N images are taken with the sinusoidal pattern shifted by distinct phase steps where, $N \geq 3$. The traditional techniques use three images with phase shifts of 0°, 120° and 240° in the sinusoidal illumination. Our analysis remains valid for this case as well as the case where the phase shifts are introduced randomly. We treat the Fourier transforms, $\hat{\mathcal{G}}_n$, of the N measured images as a system of N linear equations, $AX = B$, which can be written as,

$$\begin{bmatrix} 1 & e^{i2\phi_1} & e^{-i2\phi_1} \\ 1 & e^{i2\phi_2} & e^{-i2\phi_2} \\ . & . & . \\ . & . & . \\ 1 & e^{i2\phi_N} & e^{-i2\phi_N} \end{bmatrix}_{N\times 3} \begin{bmatrix} \frac{1}{2}\mathcal{H}_1(0,0)\mathcal{H}_2\left(f_x,f_y\right)\mathcal{G}_o\left(f_x,f_y\right) \\ \frac{1}{4}m\mathcal{H}_1(2f_o,0)\mathcal{H}_2\left(f_x,f_y\right)\mathcal{G}_o\left(f_x-2f_o,f_y\right) \\ \frac{1}{4}m\mathcal{H}_1(-2f_o,0)\mathcal{H}_2\left(f_x,f_y\right)\mathcal{G}_o\left(f_x+2f_o,f_y\right) \end{bmatrix}_{3\times 1} = \begin{bmatrix} \hat{\mathcal{G}}_1\left(f_x,f_y\right) \\ \hat{\mathcal{G}}_2\left(f_x,f_y\right) \\ . \\ . \\ \hat{\mathcal{G}}_N\left(f_x,f_y\right) \end{bmatrix}_{N\times 1} . \quad (3)$$

From Eq. (3), matrix A depends on ϕ_n, the phase shifts in each sinusoidally patterned image, which may be determined by using precision actuated, pre-calibrated translation stages which move the grid in known phase steps, or may be determined *a posteriori* using algorithms such as discussed in [18-21]. The matrix X may be obtained by using a simple singular value decomposition and pseudoinverse [23] of the matrix A and premultiplying B by that. The separated terms in matrix X are now analyzed. The term

$$I_{c1}\left(f_x,f_y\right) = \frac{1}{2}\mathcal{H}_1(0,0)\mathcal{H}_2\left(f_x,f_y\right)\mathcal{G}_o\left(f_x,f_y\right) \quad (4)$$

is similar to the conventional image but having an OTF given by

$$otf_1\left(f_x,f_y\right) = \frac{1}{2}\mathcal{H}_1(0,0)\mathcal{H}_2\left(f_x,f_y\right). \quad (5)$$

The second separated term, $(1/4)m\mathcal{H}_1(2f_o,0)\mathcal{H}_2\left(f_x,f_y\right)\mathcal{G}_o\left(f_x-2f_o,f_y\right)$, contains the valuable superresolution information from the shifted object Fourier transform. It can be sub-pixel shifted using the Fourier method from the $\left(f_x - 2f_o, f_y\right)$ coordinates back to the $\left(f_x, f_y\right)$ coordinates to obtain $(1/4)m\mathcal{H}_1(2f_o,0)\mathcal{H}_2\left(f_x+2f_o,f_y\right)\mathcal{G}_o\left(f_x,f_y\right)$. This is repeated for the third separated term to obtain $(1/4)m\mathcal{H}_1(-2f_o,0)\mathcal{H}_2\left(f_x-2f_o,f_y\right)\mathcal{G}_o\left(f_x,f_y\right)$. These two terms can be combined, giving

$$I_{c2}\left(f_x,f_y\right)=\frac{1}{4}\Big[m\mathcal{H}_1\left(2f_o,0\right)\mathcal{H}_2\left(f_x+2f_o,f_y\right)+m\mathcal{H}_1\left(-2f_o,0\right)\mathcal{H}_2\left(f_x-2f_o,f_y\right)\Big]\mathcal{G}_o\left(f_x,f_y\right), \quad (6)$$

which is treated as another component that will later be used to form the superresolved image. The OTF for I_{c2} is

$$otf_2\left(f_x,f_y\right)=\frac{1}{4}\Big[m\mathcal{H}_1\left(2f_o,0\right)\mathcal{H}_2\left(f_x+2f_o,f_y\right)+m\mathcal{H}_1\left(-2f_o,0\right)\mathcal{H}_2\left(f_x-2f_o,f_y\right)\Big]. \quad (7)$$

Similarly, to achieve superresolution in all directions in Fourier space, this process is repeated for, say, 60° and 120° rotation of the sinusoidal fringe illumination. Thereby, we extract four more component images – two having conventional image terms, given by I_{c3} and I_{c5}, having OTFs similar to otf_1, given by otf_3 and otf_5, and two component images having superresolution along their respective rotations in Fourier space, given as I_{c4} and I_{c6}, having OTFs similar to rotated versions of otf_2, given by otf_4 and otf_6. Now these 6 component images must be combined with appropriate OTF compensation in order to obtain an image having superresolution in all directions in Fourier space.

2.3 SNR analysis

Before we proceed with combining these component images, we analyze their SNR. Consider Eq. (2) for the specific case of $2\phi_n=0,\ \pi/2,\ \pi$ and $3\pi/2,$ where $\exp\left(\pm i2\phi_n\right)=1,\pm i,-1$ and $\mp i$. Let the four respective image Fourier transforms be $\hat{\mathcal{G}}_1,\ \hat{\mathcal{G}}_2,\ \hat{\mathcal{G}}_3$ and $\hat{\mathcal{G}}_4$.

For this specific case, the first noisy version of component $I_{c1},$ which contains conventional resolution information, can be obtained in closed form as

$$\begin{aligned}\hat{I}_{c1}\left(f_x,f_y\right)&=\frac{1}{4}\Big[\hat{\mathcal{G}}_1\left(f_x,f_y\right)+\hat{\mathcal{G}}_2\left(f_x,f_y\right)+\hat{\mathcal{G}}_3\left(f_x,f_y\right)+\hat{\mathcal{G}}_4\left(f_x,f_y\right)\Big]\\&=\frac{1}{2}\mathcal{H}_1\left(0,0\right)\mathcal{H}_2\left(f_x,f_y\right)\mathcal{G}_o\left(f_x,f_y\right)+\frac{1}{4}\Big[N_1\left(f_x,f_y\right)+N_2\left(f_x,f_y\right)\\&\qquad+N_3\left(f_x,f_y\right)+N_4\left(f_x,f_y\right)\Big].\end{aligned} \quad (8)$$

The signal power spectrum in this image is

$$\begin{aligned}\Phi_{S1}\left(f_x,f_y\right)&=\left\langle\left|\frac{1}{2}\mathcal{H}_1\left(0,0\right)\mathcal{H}_2\left(f_x,f_y\right)\mathcal{G}_o\left(f_x,f_y\right)\right|^2\right\rangle\\&=\frac{1}{4}\left|\mathcal{H}_1\left(0,0\right)\mathcal{H}_2\left(f_x,f_y\right)\right|^2\Phi_O\left(f_x,f_y\right),\end{aligned} \quad (9)$$

where $\Phi_O=\left\langle\left|\mathcal{G}_o\left(f_x,f_y\right)\right|^2\right\rangle$ is the object power spectrum. The OTF affecting this signal is given by Eq. (5).

The noise power spectrum is given as

$$\Phi_{N1}\left(f_x,f_y\right)=\frac{1}{16}\Big[\sigma_{N1}^2+\sigma_{N2}^2+\sigma_{N3}^2+\sigma_{N4}^2\Big]=\frac{1}{4}\sigma^2, \quad (10)$$

where σ_{Nk} is the noise variance in the image, where k = 1,2,…4, and assume that the noise realizations in these four images are statistically independent as well as have identical variances, σ^2. Therefore the power SNR for this image is given by

$$SNR_{c1} = \frac{\Phi_{S1}\left(f_x, f_y\right)}{\Phi_{N1}} = \left|\mathcal{H}_1\left(0,0\right)\mathcal{H}_2\left(f_x, f_y\right)\right|^2 \frac{\Phi_O\left(f_x, f_y\right)}{\sigma^2}. \tag{11}$$

The noisy version of the superresolution component I_{c2} is formed by computing the second and third separated overlapping terms, given by

$$\begin{aligned}\left[\mathcal{G}_1\left(f_x, f_y\right) - \mathcal{G}_3\left(f_x, f_y\right)\right] + i\left[\mathcal{G}_2\left(f_x, f_y\right) - \mathcal{G}_4\left(f_x, f_y\right)\right] &= m\mathcal{H}_1\left(-2f_o, 0\right)\mathcal{H}_2\left(f_x, f_y\right)\mathcal{G}_o\left(f_x + 2f_o, f_y\right) \\ &+ \left[N_1\left(f_x, f_y\right) - N_3\left(f_x, f_y\right)\right] \\ &+ i\left[N_2\left(f_x, f_y\right) - N_4\left(f_x, f_y\right)\right]\end{aligned} \tag{12}$$

and,

$$\begin{aligned}\left[\mathcal{G}_1\left(f_x, f_y\right) - \mathcal{G}_3\left(f_x, f_y\right)\right] - i\left[\mathcal{G}_2\left(f_x, f_y\right) - \mathcal{G}_4\left(f_x, f_y\right)\right] &= m\mathcal{H}_1\left(2f_o, 0\right)\mathcal{H}_2\left(f_x, f_y\right)\mathcal{G}_o\left(f_x - 2f_o, f_y\right) \\ &+ \left[N_1\left(f_x, f_y\right) - N_3\left(f_x, f_y\right)\right] \\ &- i\left[N_2\left(f_x, f_y\right) - N_4\left(f_x, f_y\right)\right]\end{aligned} \tag{13}$$

sub-pixel shifting them and summing them, and dividing by 4 for normalization, giving

$$\begin{aligned}\hat{I}_{c2}\left(f_x, f_y\right) = &\frac{1}{4}\left[m\mathcal{H}_1\left(2f_o, 0\right)\mathcal{H}_2\left(f_x + 2f_o, f_y\right) + m\mathcal{H}_1\left(-2f_o, 0\right)\mathcal{H}_2\left(f_x - 2f_o, f_y\right)\right]\mathcal{G}_o\left(f_x, f_y\right) \\ &+ \frac{1}{4}\left\{\left[N_1\left(f_x + 2f_o, f_y\right) - N_3\left(f_x + 2f_o, f_y\right) + N_1\left(f_x - 2f_o, f_y\right) - N_3\left(f_x - 2f_o, f_y\right)\right]\right. \\ &\left. + i\left[N_2\left(f_x + 2f_o, f_y\right) - N_4\left(f_x + 2f_o, f_y\right) - N_2\left(f_x - 2f_o, f_y\right) + N_4\left(f_x - 2f_o, f_y\right)\right]\right\}.\end{aligned} \tag{14}$$

Its signal power spectrum is

$$\begin{aligned}\Phi_{S2}\left(f_x, f_y\right) &= \left\langle\left|\frac{1}{4}\left[m\mathcal{H}_1\left(2f_o, 0\right)\mathcal{H}_2\left(f_x + 2f_o, f_y\right) + m\mathcal{H}_1\left(-2f_o, 0\right)\mathcal{H}_2\left(f_x - 2f_o, f_y\right)\right]\mathcal{G}_o\left(f_x, f_y\right)\right|^2\right\rangle \\ &= \frac{1}{16}\left|\left[m\mathcal{H}_1\left(2f_o, 0\right)\mathcal{H}_2\left(f_x + 2f_o, f_y\right) + m\mathcal{H}_1\left(-2f_o, 0\right)\mathcal{H}_2\left(f_x - 2f_o, f_y\right)\right]\right|^2 \Phi_O\left(f_x, f_y\right).\end{aligned} \tag{15}$$

The OTF affecting this signal is given by Eq. (7). The noise power spectrum is

$$\Phi_{N2}\left(f_x,f_y\right)=\frac{1}{16}\left[\left(\sigma_{N1}^{'2}+\sigma_{N2}^{'2}+\sigma_{N3}^{'2}+\sigma_{N4}^{'2}\right)+\left(\sigma_{N1}^{''2}+\sigma_{N2}^{''2}+\sigma_{N3}^{''2}+\sigma_{N4}^{''2}\right)\right]=\frac{1}{2}\sigma^2, \tag{16}$$

where $\sigma_{Ni}^{'}$ and $\sigma_{Ni}^{''}$ are the variances for the noise realizations shifted in the Fourier domain to $\left(f_x-2f_o,f_y\right)$ and $\left(f_x+2f_o,f_y\right)$ respectively and where we assume that the noise realizations shifted in the Fourier domain are statistically independent and have identical variances, σ^2. Therefore the SNR for this image component is

$$\begin{aligned} SNR_{c2} &= \frac{\Phi_{S2}\left(f_x,f_y\right)}{\Phi_{N2}} \\ &= \frac{m^2}{8}\left\|\left[\mathcal{H}_1\left(2f_o,0\right)\mathcal{H}_2\left(f_x+2f_o,f_y\right)+\mathcal{H}_1\left(-2f_o,0\right)\mathcal{H}_2\left(f_x-2f_o,f_y\right)\right]\right\|^2\frac{\Phi_O\left(f_x,f_y\right)}{\sigma^2}. \end{aligned} \tag{17}$$

From Eqs. (11) and (17), we can see that the SNR would be relatively lower as the spatial frequency, $2f_o$, of the illumination pattern increases. The illumination and imaging OTFs and the modulation contrast, *m*, are important parameters affecting SNR_{ci} for the superresolution components because they can potentially lower superresolution signal strength significantly compared to that of conventional component images.

Also affecting SNR_{ci} is the number of images used to form each component image. For instance, if $\hat{I}_{c1}$ is the average of *N* images, (where $N = 4$ in the analysis above), then the SNR for this component image would be given by $\left[N/\left(4\sigma^2\right)\right]\left|\mathcal{H}_1\left(0,0\right)\mathcal{H}_2\left(f_x,f_y\right)\right|^2\Phi_O\left(f_x,f_y\right)$.

Furthermore, the phase shifts in the sinusoidal illumination affect the signal strength in SNR_{ci}. For instance, if we have equally spaced phase shifts of 0°, 120° and 240°, only three images might be enough to obtain good signal strength. But if two of the phase shifts were nearly identical, then the signal strength would be low and we would need an additional, fourth image with a substantially different phase shift to obtain good signal strength in the component images. Therefore, the SNR for the component images is generalized to be

$$SNR_{ci}=\eta_i\left|otf_i\left(f_x,f_y\right)\right|^2\frac{\Phi_O}{\Phi_{Ni}} \tag{18}$$

where η_i is the contribution from the randomness of the phase shifts and multiple number of images used as well as from the SVD and pseudoinverse. We assumed $\eta_i=1$ in our simulations shown below. We obtain an estimate of Φ_O from the power spectrum of the object in a conventional image [24-27]. We obtain the factor Φ_{Ni} as the average power spectrum in a far corner in the Fourier transform of each component image, $\hat{I}_{ci}$, outside the extent of otf_i.

2.4 Image reconstruction

We employ a weighted Wiener-Helstrom-like deconvolution [28] of the *M* component images to combine them together,

$$I_{rec}(x,y) = IFT\left\{\sum_{i=1}^{M}\left[\frac{\hat{I}_{ci}(f_x,f_y)}{otf_i(f_x,f_y)} \times \frac{SNR_{ci}}{c + \sum_{j=1}^{M} SNR_{cj}}\right]\right\} \tag{19}$$

which is implemented using Eq. (18) as

$$I_{rec}(x,y) = IFT\left\{\sum_{i=1}^{M}\left[\frac{\hat{I}_{ci}(f_x,f_y)\,otf_i^*(f_x,f_y)\,\eta_i \frac{\Phi_O}{\Phi_{Ni}}}{c + \sum_{j=1}^{M} \eta_j \left|otf_j(f_x,f_y)\right|^2 \frac{\Phi_O}{\Phi_{Nj}}}\right]\right\}. \tag{20}$$

This is a multiframe deconvolution filter and weights each component image, $\hat{I}_{ci}$, according to its Fourier domain power SNR. We usually set the constant c = 1 which gives us a least squares solution, but lower values of c may be used for increased visual contrast at the expense of increased noise in the image. The OTF of the illumination and imaging systems are characterized to obtain $\mathcal{H}_1$ and $\mathcal{H}_2$. The modulation contrast, m, may be determined from the efficiency of the sinusoidal grating in the imaging system. We assumed a high contrast grating and set m = 1 in our simulations.

3. SIMULATION RESULTS

For our simulations we used the pristine object shown in Figure 2(a). It has fine features such as leaves, bricks, bars, etc. Many of these features are horizontal or vertical. Therefore, in Figure 2(g), in the Fourier domain of this object, we see distinct horizontal and vertical streaks which are the Fourier transforms of those horizontal and vertical features.

Figure 2(b) shows the simulated, noise-free conventional image. It has a finite extent in the Fourier domain due to the OTF as seen in its Fourier transform in Figure 2(h). Fine features of the bricks and leaves cannot be seen in this image because their spatial frequencies lie outside the passband of the conventional image in this simulation.

The OTF-compensated version of the noise-free conventional image is shown in Figure 2(c). Although its contrast is improved, its Fourier transform in Figure 2(i) shows that the OTF compensation does not increase the spatial frequency extent or add new information to it. Therefore the finest details in the bricks and leaves are still not visible in this image.

In order to perceive these fine details, one would need to extend the passband of the image. The structured illumination processing detailed in Section 2 can be used to obtain superresolution. We simulated an incoherent sinusoidal illumination with a spatial frequency at 81% of cutoff frequency. Three images for each orientation at 0˚, 60˚ and 120˚, having equally spaced, known phase shifts at 0˚, 120˚ and −120˚ were used. Random phase shifts could also have been used as demonstrated in [21]. As mentioned before, these phase shifts can be introduced in a pre-calibrated, known manner or determined *a posteriori* [18-21]. We assumed complete knowledge of the phase shifts in this image recovery. The resulting reconstruction having 81% superresolution is shown in Figure 2(d). This image shows more details such as fine features in the leaves and bricks. Its Fourier transform in Figure 2(j) clearly shows an extended passband, and the horizontal and vertical streaks in the Fourier domain are visible all the way to the edge of this extended passband. The

increase in the extent of the passband is proportional to the spatial frequency of the sinusoidal illumination and effectively the superresolution in the image. There is no noise in the structured illumination images used to obtain this reconstruction. The quality of the reconstruction deteriorates with the introduction of noise.

Gaussian noise was added to the next set of images. In Figure 2(e) we obtain a reconstruction using sinusoidally patterned images having an SNR of 124 (mean image/standard deviation of noise). This is a relatively good SNR condition for conventional images. But as shown by the SNR analysis in Section 2.3, the high spatial frequency of the sinusoidal illumination used here, i.e. at 81% of cutoff frequency, implies that the superresolution signal is significantly attenuated by the circular-aperture illumination OTF which alone contributes a factor $\left|\mathcal{H}_1\left(2f_o,0\right)\right|^2 = 0.0096$ at this frequency. This factor would be larger for a sinusoidal illumination with lower spatial frequency or if the sinusoidal pattern were produced by interfering two laser beams. Additionally, for the double-pass system we have simulated, we also have another factor of the imaging OTF, $\mathcal{H}_2$, further reducing the effective SNR of the superresolution component in this image. The noise from the structured illumination images appears as colored noise in the reconstructed superresolved image. The extended passband seen in the Fourier transform in Figure 2(k) also shows noise which is more distinct in the periphery of the extended OTF where the superresolved object transform is weaker. Therefore, in the reconstruction at this high spatial frequency of the sinusoidal illumination, we see that the superresolution is not easily evident in the image, and the finer features of the leaves and brick pattern that we seek are not distinct.

This SNR limitation can be remedied by using a greater number of composite images, with different noise realizations, to obtain a reconstruction. Figure 2(f) shows the reconstruction, having 81% superresolution, obtained from processing 10 sets of such composite images in the multiframe filter in Eq. (20). Now the fine superresolved features of the bricks and leaves are more evident than before. The Fourier domain shown in Figure 2(l) also shows that the extended horizontal and vertical streaks from the object structured are somewhat more visible in the Fourier domain of this reconstruction and the higher spatial frequencies are no longer completely drowned in noise as for the case of Figure 2(k). Fewer component images would need to be used if we were aiming for lesser values of superresolution, such as 50% of cutoff frequency.

4. CONCLUSIONS

We have analyzed the reconstruction of images to obtain lateral superresolution from sinusoidally illuminated images. We have included SNR considerations in our analysis for the combination of all superresolution and conventional image components to obtain a multiframe image reconstruction filter which adds every component image with appropriate weighting. The superresolution information is sensitive to noise and multiple images may need to be added in order to obtain effective superresolution. Simulations show up to 81% superresolution is possible even in the presence of noise. The sensitivity to noise decreases substantially for lower values of superresolution.

Our ongoing and future work in this area includes working on moving objects such as the human retina *in vivo*. We are implementing this analysis on experimental images obtained from a fluorescence microscope.

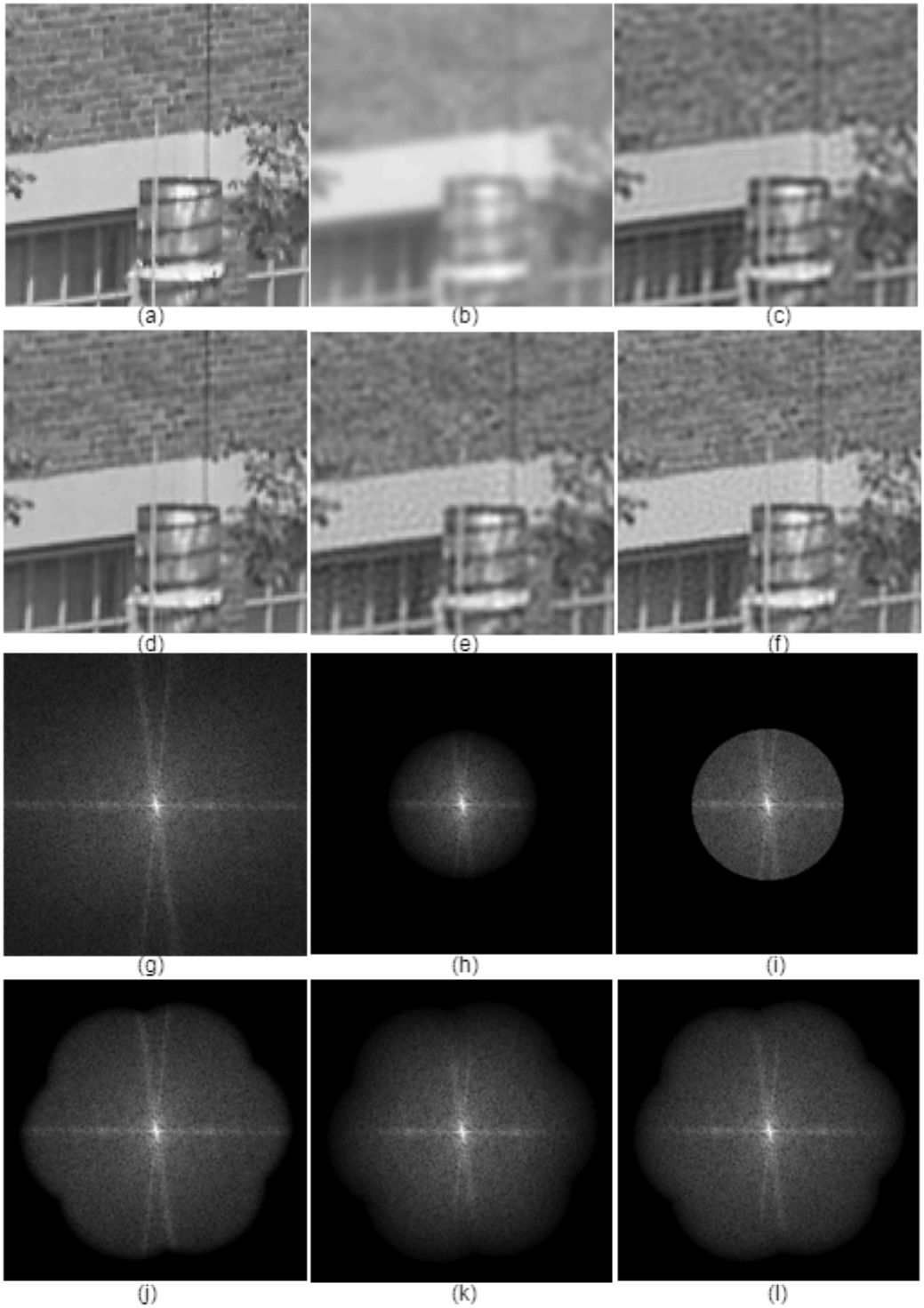

Figure 2. (a) Pristine object used in simulation, (b) conventional image, (c) OTF-compensated version of conventional image, (d) superresolved image obtained from noiseless images, (e) superresolved image obtained from noisy images (SNR = 124), (f) superresolved image obtained from noisy images (SNR = 124, used 10 sets of composite images), (g) – (l) Fourier transforms of (a) – (f) respectively. Figures 2(d) – (f) and (j) – (l) have 81% superresolution.

REFERENCES

[1] M. Gustaffson, "Surpassing the lateral resolution limit by a factor of two using structured illumination microscopy," Journal of Microscopy, Vol. **198**, Pt 2, pp 82 – 87 (May 2000).

[2] M. Gustafsson, "Extended-Resolution Reconstruction of Structured Illumination Microscopy Data," in Adaptive Optics: Analysis and Methods/Computational Optical Sensing and Imaging/Information Photonics/Signal Recovery and Synthesis Topical Meetings on CD-ROM, Technical Digest (Optical Society of America, 2005), paper JMA2.

[3] M. Gustafsson, L. Shao, D.A. Agard, J.W. Sedat, "Fluorescence microscopy without resolution limit," Biophotonics/Optical Interconnects and VLSI Photonics/WBM Microcavities, 2004 Digest of the LEOS Summer Topical Meetings , **2**, 28-30 (June 2004).

[4] R. Heintzmann, C. Cremer, "Laterally Modulated Excitation Microscopy: Improvement of resolution by using a diffraction grating," Optical Biopsies and Microscopic Techniques III, Irving J. Biglo, Herbert Schneckenburger, Jan Slavik, Katrina Svanberg, M.D., Pierre M. Viallet, Editors, Proceedings of SPIE Vol. **3568**, pp. 185 – 196 (1999).

[5] M. Gustafsson, "Extended resolution fluorescence microscopy, " Current Opinion in Strcutural Biology, **9**:627 – 634 (1999).

[6] W. Lukosz, "Optical sytems with resolving powers exceeding the classical limits II," J. Opt. Soc. Am **57**, 932- 941 (1967).

[7] D. Mendlovic, A. W. Lohmann, N. Konforti, I. Kiryuschev, and Z. Zalevsky, "One-dimensional superresolution optical system for temporally restricted objects ," Appl. Opt. **36**, 2353-2359 (1997).

[8] E. Sabo, Z. Zalevsky, D. Mendlovic, N. Konforti, and I. Kiryuschev, "Superresolution optical system using three fixed generalized gratings: experimental results," J. Opt. Soc. Am. A **18**, 514-520 (2001).

[9] A. Shemer, Z. Zalevsky, D. Mendlovic, N. Konforti, and E. Marom, "Time Multiplexing Superresolution Based on Interference Grating Projection ," Appl. Opt. **41**, 7397-7404 (2002).

[10] S. W. Hell and J. Wichmann, "Breaking the diffraction resolution limit by stimulated emission: stimulated-emission-depletion fluorescence microscopy," Opt. Lett. **19**, 780- (1994).

[11] X. Chen and S. R. J. Brueck, "Imaging interferometric lithography: approaching the resolution limits of optics," Opt. Lett. **24**, 124-126 (1999).

[12] C. J. Schwarz, Y. Kuznetsova, and S. R. J. Brueck, "Imaging interferometric microscopy ," Opt. Lett. **28**, 1424-1426 (2003).

[13] V. Mico, Z. Zalevsky, and J. García, "Superresolution optical system by common-path interferometry," Opt. Express **14**, 5168-5177 (2006).

[14] G. E. Cragg and P. T. C. So, "Lateral resolution enhancement with standing evanescent waves ," Opt. Lett. **25**, 46-48 (2000).

[15] E. Chung, D. Kim, and P. T. So, "Extended resolution wide-field optical imaging: objective-launched standing-wave total internal reflection fluorescence microscopy," Opt. Lett. **31**, 945-947 (2006).

[16] M. A. A. Neil, R. Juskaitis, and T. Wilson, "Method of obtaining optical sectioning by using structured light in a conventional microscope," Opt. Lett. **22**, 1905-1907 (1997).

[17] Neil et al., 1998 M.A.A. Neil, R. Juškaitis and T. Wilson, Real time 3D fluorescence microscopy by two beam interference illumination, *Opt. Commun.* **153** (1998), pp. 1–4.

[18] L. H. Schaefer, D. Schuster, J. Schaffer, "Structured illumination microscopy: artefact analysis and reduction utilizing a parameter optimization approach," Journal of Microscopy **216**:2, 165-174 (2004).

[19] S. A. Shroff, J. R. Fienup, and D. R. Williams, " Phase Shift Estimation in Structured Illumination Imaging for Lateral Resolution Enhancement," in *Adaptive Optics: Analysis and Methods/Computational Optical Sensing and Imaging/Information Photonics/Signal Recovery and Synthesis Topical Meetings on CD-ROM*, OSA Technical Digest (CD) (Optical Society of America, 2007), paper SMA2.

[20] S. A. Shroff, J. R. Fienup, and D. R. Williams, "Estimation of Phase Shifts in Structured Illumination for High Resolution Imaging," in *Frontiers in Optics*, OSA Technical Digest (CD) (Optical Society of America, 2007), paper FMH4.

[21] S. A. Shroff, J. R. Fienup and D. R. Williams, "Phase-Shift Estimation in Sinusoidally Illuminated Images for Lateral Superresolution," J. Opt. Soc. Am. A, submitted (2008).

[22] P. Artal, S. Marcos, R. Navarro, and D. R. Williams, "Odd aberrations and double-pass measurements of retinal image quality," J. Opt. Soc. Am. A **12**, 195- (1995).

[23] G. Strang, *Linear Algebra and Its Applications* (Thomson Learning, Inc. 1998).
[24] D. J. Tolhurst, Y. Tadmore, and T. Chao, "Amplitude spectra of natural images," Ophthal. Physiol. Opt. **12**, 229-232 (1992).
[25] A. van der Schaaf and J. H. van Hateren, "Modelling the power spectra of natural images: statistics and information, " Vision Res. **36**, 2759-2770 (1996).
[26] D. R. Gerwe, M. Jain, B. Calef, and C. Luna, "Regularization for nonlinear image restoration using a prior on the object power spectrum," in Unconventional Imaging, Proc. SPIE **5896**, 1-15 (2005).
[27] J. R. Fienup, D. Griffith, L. Harrington, A. M. Kowalczyk, J. J. Miller, and J. A. Mooney, "Comparison of reconstruction algorithms for images from sparse-aperture systems," in Image Reconstruction from Incomplete Data II, P. J. Bones, et al., eds., Proc. SPIE 4792, 1-8 (2002).
[28] L. P. Yaroslavsky and H. J. Caulfield, "Deconvolution of multiple images of the same object," Appl. Opt. **33**, 2157-(1994).